Geochemistry Geophysics Geosystems G3

Published by AGU and the Geochemical Society

Article
Volume 14, Number 4
24 April 2013
doi:10.1029/2012GC004440
ISSN: 1525-2027

Measuring the Curie temperature

K. Fabian
Geological Survey of Norway, Leiv Eirikssons vei 39, Postboks 6315 Sluppen, 7491 Trondheim, Norway (karl.fabian@ngu.no)

V. P. Shcherbakov
Geophysical Observatory 'Borok', Yaroslavskaja Oblast, 151742, Russia

S. A. McEnroe
Department of Geology and Mineral Engineering, NTNU Trondheim, 7491 Trondheim, Norway

[1] Curie point temperatures (T_C) of natural and synthetic magnetic materials are commonly determined in rock magnetism by several measurement methods that can be mutually incompatible and may lead to inconsistent results. Here the common evaluation routines for high-temperature magnetization and magnetic initial susceptibility curves are analyzed and revised based on Landau's theory of second-order phase transitions. It is confirmed that in high-field magnetization curves T_C corresponds to the inflection point, below the temperature of maximum curvature or the double-tangent intersection point. At least four different physical processes contribute to the initial magnetic susceptibility near the ordering temperature. They include variation of saturation magnetization, superparamagnetic behavior, magnetization rotation, and magnetic domain wall motion. Because each of these processes may influence the apparent position of T_C, initial susceptibility and high-field curves can yield deviating estimates of T_C. A new procedure is proposed to efficiently determine the temperature variation of several magnetic parameters on a vibrating-sample magnetometer, by repeatedly measuring quarter-hysteresis loops during a single heating cycle. This procedure takes measurements during the inevitable waiting time necessary for thermal equilibration of the sample, whereby it is not slower than the commonly performed measurements on a Curie balance. However, it returns saturation magnetization, saturation remanence, high-field and low-field slopes, and other parameters as a function of temperature, which provide independent information about T_C and other sample properties.

Components: 7,400 words, 9 figures.

Keywords: rock magnetism; paleomagnetism.

Index Terms: 1519 Magnetic mineralogy and petrology; 1540 Rock and mineral magnetism; 1594 Instruments and techniques.

Received 17 September 2012; **Revised** 28 November 2012; **Accepted** 29 November 2012; **Published** 24 April 2013.

Fabian K., V. P. Shcherbakov and S. A. McEnroe (2013), Measuring the Curie temperature, *Geochem. Geophys. Geosyst.*, *14*, 947–961, doi:10.1029/2012GC004440

1. Introduction

1.1. Curie Point Determination in Rock Magnetism

[2] The Curie, or Néel temperature of a ferromagnetic or ferrimagnetic, or antiferromagnetic material, is the temperature where its uncompensated spins in zero-field undergo a second-order phase transition from a thermally disordered high-temperature to a magnetically ordered low-temperature state. For simplicity, we here follow the practice of *Petrovský and Kapička* [2006] and use the term *Curie point temperature* (T_C) to denote all cases. The measurement of T_C is one of the central techniques in rock magnetism. In most applications it is a fast, reliable, and well-proven method to determine the predominant magnetic minerals in natural or synthetic samples, even if their concentrations are small. This is so for several reasons:

1. Magnetic measurements are very sensitive, and the presence or absence of magnetic signals are very easily and precisely detectable.
2. The two most common natural magnetic oxides have clearly distinct Curie points: magnetite at 580°C, and hematite at 680°C [*Petersen and Bleil*, 1982].
3. Within the common natural solid-solution series of magnetic minerals, titanomagnetites, titanomaghemites, titanohematites, and ferri-ilmenites, the Curie point temperature varies over a wide temperature range and can be used to tightly constrain the magnetic-mineral composition or oxidation state [*Petersen and Bleil*, 1982].

[3] Because magnetic measurements are very sensitive, the onset of magnetic ordering can be observed using different magnetic measurement parameters, like static in-field magnetization, or AC-susceptibility. In both cases the transition from a less magnetized to a more magnetized state within a relatively small temperature interval is observed and correctly interpreted as resulting from the magnetic ordering that takes place when crossing the Curie point during cooling. However, there is no clear practical agreement about the accurate position of T_C within this temperature interval that for magnetite easily covers from 10°C up to 30°C or more. This usually is of minor importance, e.g., when the value of T_C is used to distinguish between magnetite and hematite, or when the measurement should yield an average estimate for the composition of a titanomagnetite. However, when a precise composition determination is needed, or when two phases coexist with very close Curie point temperatures, inconsistent measurement methods for T_C can lead to severely misleading conclusions. The aim of this article is to clarify the theoretical background of different approaches presently used to measure the Curie point temperature, and in addition to propose a new experimental protocol to reliably determine an accurate value of T_C using a high-temperature vibrating-sample magnetometer (VSM).

1.2. Common Methods for Curie Point Determination

[4] There are several types of instruments in use to determine approximate Curie point temperatures. An overview of the different methods to determine $M_s(T)$-curves can be found in *Collinson* [1993]. In a Curie balance, a field—typically between $\mu_0 H_{ex}$=0.1 T and 1 T—is generated in a small area, leading to a strong field gradient that draws ferromagnetic and paramagnetic substances toward the stronger magnetic field, while diamagnetic substances are repulsed. This force is then precisely compensated by an additional coil. The current required for this compensation is proportional to the magnetization of the sample in the external field H_{ex}. Ferromagnets (and also ferrimagnets) are paramagnetic above T_C and still carry an induced magnetization. Most natural samples also contain other paramagnetic minerals contributing a magnetization $\chi_p(T)H_{ex}$ that is considered as a major source of smoothing of the transition [e.g., *Tauxe*, 1998]. Two other possible smoothing mechanisms are inhomogeneity of the ferrimagnetic material and a temperature gradient inside the sample. Both effects lead to a smoothing of the transition due to an apparent or real distribution of Curie point temperatures as sketched in Figure 1. To obtain the correct Curie points from such smoothed measurements, a number of different methods have been suggested and used in the rock magnetic literature.

[5] *Ade-Hall et al.* [1965] used a Chevallier torsion balance for measuring the induced magnetization in 0.1 T. They introduced the "practical definition" of the Curie point T_C, as the "temperature at which the curvature of the concave part of the heating curve is a maximum". In view of our theoretical considerations below, their justification for this definition is interesting: "The point of inflection was far too poorly defined to provide a practical Curie point" [*Ade-Hall et al.*, 1965]. This method of maximum curvature is now one of the two most common methods used to determine T_C in rock magnetism [e.g., *Tauxe*, 1998; *Leonhardt*, 2006; *Lagroix et al.*, 2004].

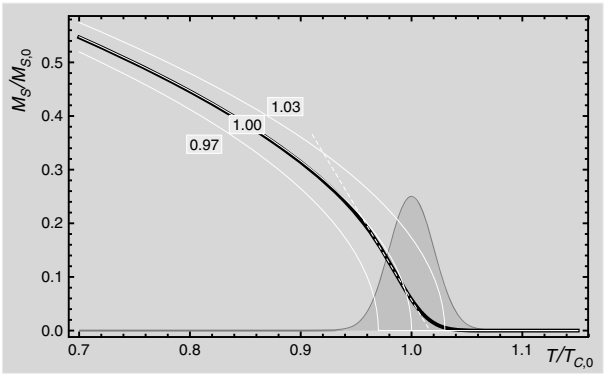

Figure 1. The concept behind determining the Curie point by maximum curvature or two-tangent crossing. The theoretically sharp transition at $T/T_{C,0}$ is smoothed by inhomogeneities in either composition or temperature of the material. In addition, paramagnetic magnetization from the substance itself or from matrix minerals can further diffuse the transition. Also, magnetization offsets from ordered phases with a higher T_C do commonly occur. The figure shows how a distribution (shaded distribution) of ideal $M_S(T)$-curves (white lines) with slightly different T_C values lead to a smoothed average curve (black line). A more comprehensive concept is developed in the text.

[6] The other very common method is the two-tangent method, initially described by *Grommé et al*. [1969]: "Curie points were determined by drawing straight lines approximately coinciding with the *J*–*T*-curve respectively above and below the estimated Curie point, and projecting their intersection to the temperature axis." They do not give a physical argument for this method, but point out that they individually chose the external field H_{ex} between 140 and 400 mT to coincide with the "knee" of the *J*–*H*-curve of the sample—probably measured at room temperature—in order to avoid unnecessary large induced magnetization from paramagnetic substances in the sample.

[7] To devise a physically based method to determine Curie points for irreversible heating curves of titanomaghemites, *Moskowitz* [1981] analyzed the graphical two-tangent method and proposed a new extrapolation method that is based on the Landau theory of second-order phase transitions, and provides an estimate of T_C by using only data acquired below T_C. A drawback of this approach is that it essentially uses the absolute value of the magnetization, and therefore can only be used for the highest Curie point temperature occurring in the sample.

[8] This disadvantage also applies to the *Arrott plot*, which is based on a molecular-field approximation of the free energy as a function of spontaneous magnetization, and widely used in physics to determine the Curie point of pure substances [*Arrott*, 1957; *Arrott and Noakes*, 1967]. A general introduction is found in *Bertotti* [1998] (section 5.1.3).

[9] Curie point temperatures have also been determined from curves of temperature-dependent magnetic initial susceptibility $\chi_0(T)$. The importance of the difference between determining T_C from $M_s(T)$ and $\chi_0(T)$ is pointed out by *Petrovský and Kapička* [2006], where methods to determine T_C from measurements of the initial susceptibility are analyzed. They conclude that the two-tangent method is not suitable for $\chi_0(T)$ and can considerably overestimate T_C.

[10] The physical origin of $\chi_0(T)$ close to T_C is more challenging than that of $M_s(T)$, because a number of low-field effects are important for $\chi_0(T)$, but become negligible in the higher fields used to infer $M_s(T)$. The variation of m depends not only on the variation of $M_s(H,T)$ with field H, it also contains a contribution from a rotation of the ordered moment with respect to an easy magnetization axis, and contributions from thermally activated switching of small independent – but already magnetically ordered – regions (e.g., SP particles). In large bulk material domain-wall movement contributes to $\chi_0(T)$ even slightly below T_C. In nanoparticles the inhomogeneity of M_S, due to the different exchange coupling of inner and surface atoms, is of additional importance.

1.3. Toward Unifying Theory and Experiment in Curie Point Determination

[11] In this article, we focus on the behavior of $M_s(T)$ and $\chi_0(T)$ of bulk material, where magnetic long-range order can develop without significant influence from particle boundaries and interfaces. Variation of T_C and $M_s(T)$ with particle size is relevant for nanoparticles only [*Shcherbakov et al*., 2012].

2. The Curie Point Temperature in Landau Theory With Field Term

[12] The study of the magnetic phase transition at the Curie point is commonly formulated in terms of the Landau theory based on the approximate fourth-order expansion of the zero-field free energy near T_C in terms of the order parameter $m = M_s(T)/M_s(0)$, which yields

$$F = F_0 + bm^4 + a\tau m^2. \quad (1)$$

[13] Here $\tau = (T - T_C)/T_C$, F_0 is constant, and a, $b > 0$. Due to the time inversion symmetry of the Maxwell equations, F contains no odd terms in m. At the minima of F one has $dF/dm = 0$, $d^2F/dm^2 > 0$ and therefore

$$|m| = \sqrt{\frac{a}{2bT_C}}(T_C - T)^{1/2}\ [T < T_C], \quad (2)$$

where the Iverson bracket $[X]$ is defined to be one, if the logical statement X is true, and zero otherwise. This characteristic square root behavior of $m(T)$ apparently sharply defines T_C. Unfortunately, this result is based on the absence of external fields, even though it has traditionally been used to interpret data from measurements performed within external fields of considerable strength. In the full Landau theory [e.g., *Landau and Lifshitz*, 1980, chap. 144], the field energy $-mH$ is explicitly taken into account and the free energy becomes

$$F = F_0 + bm^4 + a\tau m^2 - mH. \quad (3)$$

[14] The condition $dF/dm = 0$ leads to

$$4bm^3 + 2a\tau m = H. \quad (4)$$

[15] By rescaling m and H to $m_{scaled} = \sigma m$ with $\sigma^2 = 2b/a$, and $h = \sigma/(2a)H$ the equation becomes

$$m^3 + \tau m = h. \quad (5)$$

[16] After rescaling, the derivatives m', m'' of m with respect to τ fulfill the equations

$$3m^2m' + m + \tau m' = 0. \quad (6)$$

and

$$3m^2m'' + 6m(m')^2 + 2m' + \tau m'' = 0. \quad (7)$$

[17] At an inflection point with $m'' = 0$ and $m' \neq 0$ the last equation yields $3\ mm' = -1$, which if substituted into (6) yields $\tau = 0$.

[18] This implies that within an external field, the Curie point corresponds to the temperature where the magnetization curve has an inflection point with $m'' = 0$. This also is the minimum of the derivative m'. The theoretical predictions from Landau theory are plotted for different normalized fields h in Figure 2. Note that in case of $h \neq 0$ there is no second-order phase transition from a disordered to an ordered state anymore, because only for $h = 0$ the magnetization m has a discontinuity of its first derivative at $\tau = 0$. Within an external field, the condition $m'' = 0$ rather marks a crossover from a field-ordered to an exchange-ordered state, which develops into a phase transition when the field is removed.

[19] The methods of linear extrapolation or maximum curvature, which are commonly used in geophysics, are inspired by the zero-field analysis (2) and result in too high estimates of T_C when applied to in-field measurements. At the Curie point $\tau = 0$ one obtains from (5) the scaling relation

$$m = h^{1/3}. \quad (8)$$

[20] This relation can be used for a precise determination of T_C by either plotting m^3 versus h in the *Arrott plot* [*Arrott*, 1957], which is widely used in physics to determine T_C for pure materials, or by plotting m^3/h as a function of h for different temperatures, and choosing the temperature where for high h the plot best approaches a constant value m^3/h. A method equivalent to the Arrott plot was used in *Moskowitz* [1993] to determine T_C for synthetic titanomagnetites. The main disadvantage of this method is that admixtures of other magnetic minerals destroy the scaling relation (8).

[21] Calculating the derivative d/dh in (5) yields for the inverse of the susceptibility $\chi = dm/dh$ the relation

$$1/\chi = 3m^2 + \tau. \quad (9)$$

[22] This relation predicts a singularity of the initial susceptibility exactly at T_C. Generalizations of this equation, e.g., for ferrimagnets [*Néel*, 1948], predict a similar peak. Yet, experimental data show that low-field, or initial susceptibility $\chi_0(T)$ typically has a step-like shape with a sharp decrease near or at T_C on heating. A remnant of the above theoretical peak, which here will be denoted as *Landau peak*, is often only observed for the high-field slope χ_{hf}. To understand this behavior, it is necessary to extend the free-energy expression (1) by an anisotropy-energy term that describes an additional degree of freedom for the ordered magnetic moment, namely a rotation away from its easy axis. This and other additional susceptibility mechanisms are discussed in the next section.

3. Initial Susceptibility Near the Curie Point

[23] Close to the ordering temperature, the magnetic initial susceptibility $\chi_0(T)$ is influenced by

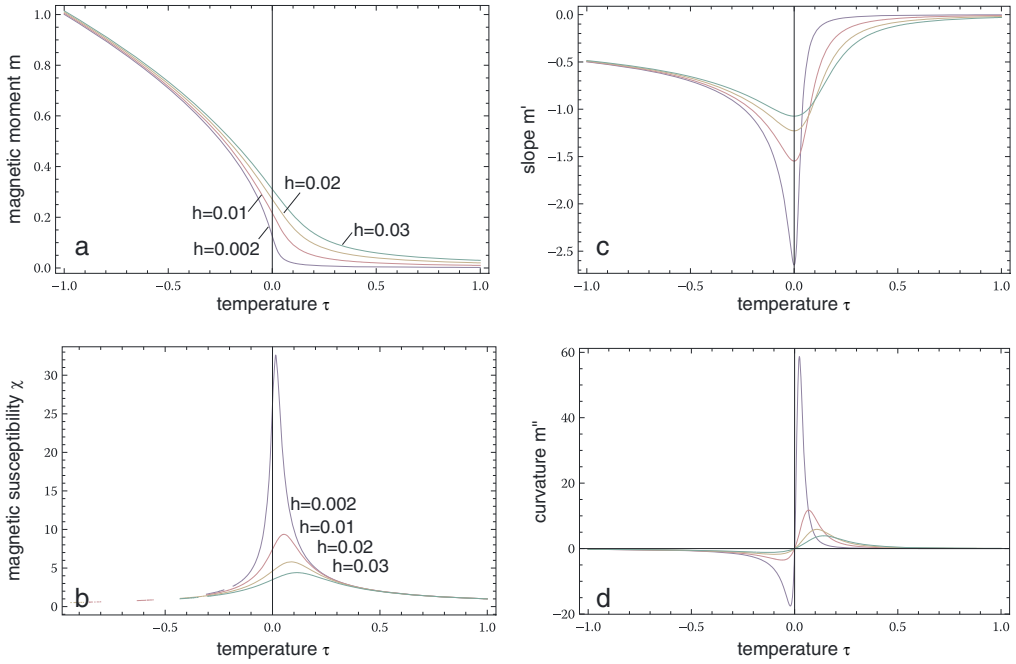

Figure 2. Plots of (a) magnetic moment $m(\tau)$, (b) susceptibility $\chi(\tau)$, (c) slope $m'(\tau)$, and (d) curvature $m''(\tau)$ as a function of normalized field h temperature τ for the phase transition in the scaled Landau theory. The Curie point at $\tau = 0$ corresponds for nonzero field values h to the point of steepest slope, which is the minimum of $m'(\tau)$, or the zero of $m''(\tau)$. The point of maximum curvature shifts toward higher temperature with increasing external field h. Also, the maximum of in-field magnetic susceptibility lies above the Curie point. In small fields, magnetic susceptibility has a sharp peak almost at $\tau = 0$.

several independent mechanisms by which a small applied field generates a magnetization along the field axis. To classify these, it is assumed that a thermally stable magnetic particle with total volume v, and saturation magnetization M_s contains a number of magnetic phases with volumes v_i and magnetization directions $\mathbf{m}_i$. At zero field almost all phases correspond to magnetic domains aligned with easy anisotropy axes. The total magnetization then is

$$M = \frac{1}{v}\sum_i M_s v_i \mathbf{m}_i, \tag{10}$$

whereby the susceptibility contains the three terms

$$\frac{dM}{dH} = \frac{1}{v}\sum_i \left(\frac{dM_s}{dH} v_i \mathbf{m}_i + M_s \frac{dv_i}{dH}\mathbf{m}_i + M_s v_i \frac{d\mathbf{m}_i}{dH}\right). \tag{11}$$

[24] The first term represents the change of M_s with field (para-effect), the second term represents domain wall motion and the corresponding change in domain volumes. The third term represents rotation of magnetization directions within the domains against magnetic anisotropy. At high temperatures above T_C, exchange couplings between atoms are small in comparison to thermal energy, and the individual atoms react to an external field through the mechanisms of diamagnetism and paramagnetism. Near, but below T_C, the whole particle volume is only one magnetic domain, and because thermal energy dominates, its direction behaves paramagnetically, and magnetic anisotropy is less effective. This is the superparamagnetic state with its associated susceptibility. These main physical mechanisms of magnetic susceptibility are sketched in Figure 3, and below will be discussed separately with respect to their influence upon the determination of T_C. Their relative contributions at a specific temperature depend on the grain-size distribution within the sample. Accordingly, the shape of the magnetic susceptibility curve strongly depends on grain size.

3.1. Susceptibility Due to Variation of $M_s(H)$

[25] The first term on the right-hand side of (11) describes the so-called *para-effect* due to the variation dM_s/dH at a fixed temperature [*Holstein and Primakoff*, 1940]. Physically, it results from the fact that below T_C the saturation magnetization in

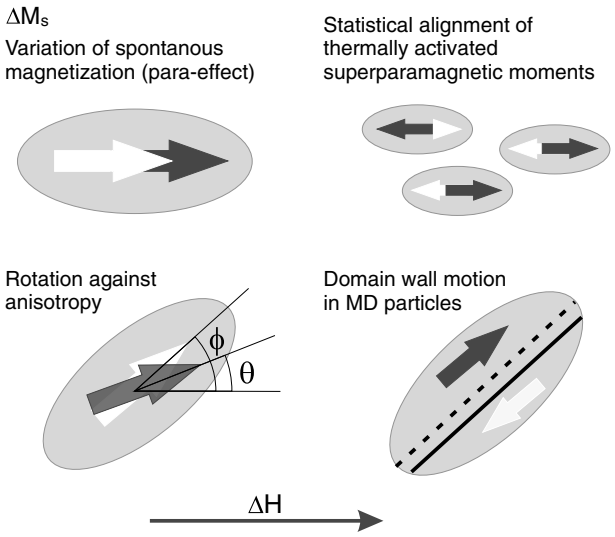

Figure 3. Four independent mechanisms of magnetic susceptibility in a ferrimagnet as discussed in the text. When increasing the field by a vector ΔH the magnetic moment aligned with this direction (black) also increases as compared to the initial or opposite magnetization (white). The different mechanisms are: (a) Field-induced change of M_s (para-effect), (b) superparamagnetism, (c) rotation against anisotropy, where ϕ denotes the angle of the field to an easy axis, and θ the deflection of the moment due to the applied field. (d) Domain wall motion in multidomain particles.

zero field represents an equilibrium between exchange coupling and thermal activation. The average spin contributed to M_s by a magnetic ion like Fe^{3+} is lower than its theoretical value at $T = 0$ K. By applying a field, the coupling between neighboring spins is effectively enhanced which shifts the equilibrium to increased spin alignment and in turn also increases M_s. In Landau theory the para-effect is implicitly described by equation (5), and Figure 2b shows that only close to T_C it contributes noticeably to $\chi_0(T)$. According to (9), χ_0 has a singularity at T_C, where τ and m are zero. This singularity is effectively suppressed in any finite applied field, even in those used for measuring χ_0. The para-effect therefore is not necessarily recognized in real measurements of $\chi_0(T)$, where other susceptibility mechanisms are more prominent. However, the increase of $M_s(H)$ with field still occurs at high fields, where all other mechanisms are saturated, whereby the para-effect can generate a clear Landau peak of high-field susceptibility $\chi_{hf}(T)$ slightly above T_C, which is in accordance with Figure 2b. Note that within a field, M_s is nonzero even above T_C, because the field cooperates with the exchange coupling. Inserting (8) into (9) yields exactly at T_C the relation $\chi_{hf}(h) \propto h^{-2/3}$. The general analysis by *Holstein and Primakoff* [1940] otherwise gives $\chi_{hf}(h) \propto h^{-1/2}$.

3.2. Susceptibility Due to Anisotropy

[26] A significant contribution to $\chi_0(T)$ just below T_C is rotation of a single-domain magnetic moment against magnetic anisotropy (Figure 3c). By this mechanism $\chi_0(T)$ maintains a high value on cooling. Magnetic anisotropy defines preferred magnetization directions (easy axes) for the ordered spins in zero field, and can be due to either crystallographic anisotropy, or shape anisotropy, whereby the latter arises from the self-demagnetizing effect in elongated single-domain particles. Applying a field rotates the spins away from its easy axis, thereby providing a susceptibility mechanism even when there is no change in M_s.

[27] For a theoretical treatment, one can extend the Ginzburg-Landau theory from the previous section. The mean magnetic moment per atom is $M = mS\mu_B$, where S is the spin quantum number, and μ_B the Bohr magneton. The uniaxial anisotropy energy from shape anisotropy per atom contributes an energy $K(\mathbf{m}) = km^2\sin^2(\phi - \theta)$, where ϕ denotes the angle between easy axis and field direction, and $\theta \leq \phi$ denotes the angle between field and mean magnetization vector $\mathbf{m}$. The modified Landau free energy per atom thereby becomes

$$F = \frac{a\tau}{2}m^2 + \frac{b}{4}m^4 + Km^2\sin^2(\phi - \theta) - mS\mu_B H\cos\theta. \tag{12}$$

[28] To estimate the relative size of these terms, *Shcherbakov et al.* [2012] use a mean-field approximation of the Heisenberg Hamiltonian to obtain an approximation F_{mf} for the free energy F, which results in

$$F_{\mathrm{mf}} = k_B T_C \frac{3S\tau}{2(1+S)}m^2 + k_B T_C \frac{9S(1+2S(1+S))}{40(1+S)^3}m^4. \tag{13}$$

[29] The normalized parameters a and b are therefore

$$\alpha = \frac{a}{k_B T_C} = \frac{3S}{1+S}, \tag{14}$$

$$\beta = \frac{b}{k_B T_C} = \frac{9S(1+2S(1+S))}{10(1+S)^3}. \tag{15}$$

[30] Equation (12), after division by $k_B T_C$ therefore yields

$$f = \frac{F}{k_B T_C} = \frac{\alpha\tau}{2} m^2 + \frac{\beta}{4} m^4 + \frac{k}{2} m^2 \sin^2(\phi - \theta) - mh \cos\theta. \tag{16}$$

[31] Here the normalized material and field parameters are

$$k = \frac{2K}{k_B T_C}, \tag{17}$$

and

$$h = \frac{S\mu_B H}{k_B T_C}. \tag{18}$$

[32] A realistic order of magnitude for the rescaled anisotropy constant k and field h can be estimated. For magnetite the shape anisotropy constant at room temperature is approximately $\mu_0 M_s^2 \approx 3 \cdot 10^4$ J/m^3 and $k_B T_C \approx 1.2 \cdot 10^{-20}$ J/atom. The magnetite unit-cell contains $3Z/2 = 12$ pairs of Fe atoms—or ferrimagnetic moments—and has volume $V \approx 5.91 \cdot 10^{-28}$ m^3. In combination, this results in $k \approx 2 \cdot 10^{-5}$. On the other hand, an external field of $B = 1$ mT corresponds to $h \approx 2 \cdot 10^{-7}$.

[33] For a given angle $\phi \in [0, \pi/2]$, minimization of (16) with respect to θ and m results in the equations

$$\frac{\partial f}{\partial m} = \alpha\tau m + \beta m^3 + km \sin^2(\phi - \theta) - h \cos\theta = 0, \tag{19}$$

$$\frac{\partial f}{\partial \theta} = \frac{k m^2}{2} \sin 2(\theta - \phi) + m h \sin\theta = 0. \tag{20}$$

[34] Clearly, for $h = 0$, $m = 0, \theta = \phi$ is a solution, which becomes unstable at $\tau = 0$, where $\partial^2 F / \partial m^2$ changes sign. For the region, where $\tau < 0$, these equations cannot be solved analytically, but numerical solutions can be readily found. The resulting magnetization curve depends on the relative values of h and k (Figure 4). If $km \ll h$, which for constant h applies somewhere in the vicinity of T_C, then $\theta \approx 0$, and the magnetization is directed along the field direction. In this case anisotropy is negligible, and (19) and (20) reduce to the pure Landau theory, where $m = \sqrt{\alpha\tau/\beta}$, such that $h > km$ is equivalent to $\tau < \beta/\alpha(h/k)^2$. Because $k(\tau)$ vanishes rapidly near T_C, for constant h there always is a temperature range close to T_C, where anisotropy is negligible and $m(\tau,h)$, and accordingly the susceptibility measured with a constant amplitude, follows pure Landau theory. For lower temperature and small field the situation is more interesting. For example, at $h/k \approx 0.01$, and sufficiently low temperature, m is almost constant; however, its direction changes. Its component along the field follows from (19), and for a small field with $h \ll km$ one obtains

$$\phi - \theta \approx \frac{h \sin\theta}{km}. \tag{21}$$

[35] The observed magnetization projection on the field direction, m_{obs}, can then be estimated by

$$m_{obs} = m\cos\theta \approx m\cos\phi + \frac{h\sin^2\theta}{k}. \tag{22}$$

[36] By integrating this over a constant random distribution of easy axes, the first term averages to zero. For the second term the fact that $\phi - \theta$ is small implies by (21) that

$$\sin^2\theta \approx \sin^2\phi - \frac{h}{km} \sin 2\phi \sin\phi, \tag{23}$$

and the susceptibility due to rotation is obtained as

$$\chi_0^{rot} = \frac{m_{obs}}{h} \approx \frac{2}{3k}, \tag{24}$$

where the dependence of M_s on h due to the para-effect has been neglected. Otherwise, the approximation agrees with the exact calculation in the appendix, that yields for $T < T_C$ or $\tau < 0$

$$\chi_0 = -\frac{1}{6\alpha\tau} + \frac{2}{3k}. \tag{25}$$

[37] This result shows that the rotational initial susceptibility near T_C creates the characteristic step function, which is often observed as a prominent feature in measurements of initial susceptibility as a function of temperature.

3.3. Susceptibility Due to Domain Wall Motion

[38] In case of large crystals of a soft magnetic material, domain-wall motion could contribute to the initial susceptibility in the vicinity of T_C. Some

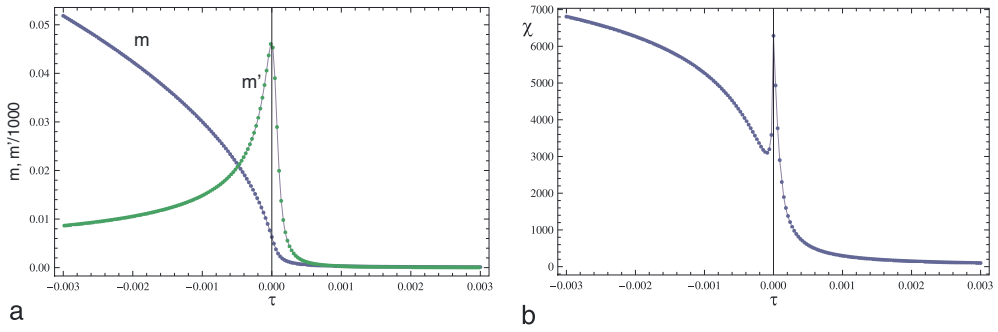

Figure 4. Magnetic moment m, and slope m' (a), as well as low-field susceptibility χ_0, as a function of normalized temperature $\tau = T/T_C - 1$ and normalized field h for the phase transition in the scaled Landau theory with anisotropy term. The normalized Curie point lies at $\tau = 0$, the normalized values for the model calculations are $S = 5/2$, implying $a \approx 2.14$ and $b \approx 0.97$, $k = 10^{-5}$ and $h = 10^{-6}$. The plots show spherical averages over all angles ϕ for an isotropic distribution of easy axes.

models show that the initial susceptibility χ_{dw} due to domain wall motion is proportional to $M_s(T)/\sqrt{K(T)}$, where $K(T)$ denotes the magnetocrystalline anisotropy constant [*Träuble*, 1966]. At high temperatures magnetostrictive effects and magnetization rotation constrain this susceptibility. For large magnetite particles of size d one can assume that classical domain wall movement can occur only if the wall thickness $\delta \approx 3\sqrt{A/K} \ll d$. Because for magnetite $A(T) \propto M_s(T)^2$, and $K(T) \propto M_s(T)^{12}$ [*Fletcher and O'Reilly*, 1974] the total effect of domain wall motion can be written as

$$\chi_{dw}(T) = \chi_{dw,0}\left[\delta_0 \frac{m_s(T)}{\sqrt{k(T)}} \ll \mathrm{d}\right] \frac{m_s(T)}{\sqrt{k(T)}} \qquad (26)$$

where $m_s(T) = M_s(T)/M_s(0)$, $k(T) = K(T)/K(0)$, δ_0 is the domain wall width, $\chi_{dw,0}$ the domain wall susceptibility at $T = 0$ K, and $[\ldots]$ again is the Iverson bracket. As long as there are domain walls in the particles, the demagnetizing effect further reduces the externally measured apparent susceptibility χ_a with respect to the internal susceptibility χ_{dw} through

$$\chi_a(T) = \frac{\chi_{dw}}{1 + N_d\,\chi_{dw}}, \qquad (27)$$

where $N_d \approx 1/3$ is an average demagnetizing factor [*Dunlop and Özdemir*, 1997, equation (9.4)]. The fact that χ_{dw} is set to zero above a critical nucleation temperature does not necessarily mean that the experimentally determined susceptibility changes substantially. It only means that domain wall motion is no longer the predominant mechanism by which the particle responds to field variations. When the domain-wall width δ becomes comparable to the grain size, the grain can no longer host multiple domains and different magnetization structures form. One of the possible configurations is a vortex structure [*Williams and Dunlop*, 1989] positioned approximately in the center of the particle, such that the net magnetization is about zero for $h = 0$. Micromagnetic calculations indicate that the susceptibility due to spin motions in a vortex state with fixed central axis is comparable to that from other susceptibility mechanisms for a field applied along the vortex axis [*Heider et al.*, 1996], and that the exchange energy for platelets is practically insensitive to the movement of the vortex axis during the initial stage of the magnetization process under the action of the external field [*Scholz et al.*, 2003; *Shcherbakov and Winklhofer*, 2010], which means that the apparent susceptibility of the vortex structure essentially follows equation (27).

[39] Figure 5a shows that the width of a 180° Bloch wall for magnetite increases very strongly as a function of temperature. Consequently, only very large particles may show a contribution of χ_{dw} near T_C, as indicated in Figure 5b. Therefore, domain wall motion is of little importance near T_C, but for large particles it leads to a noticeable susceptibility below T_C that decays toward lower temperatures as the anisotropy $|K(T)|$ increases.

3.4. Susceptibility Due to Superparamagnetism

[40] A third influence upon $\chi_0(T)$ is due to the superparamagnetic behavior of small particles. This effect has two components, both of which can be extremely important. If the particle size of the

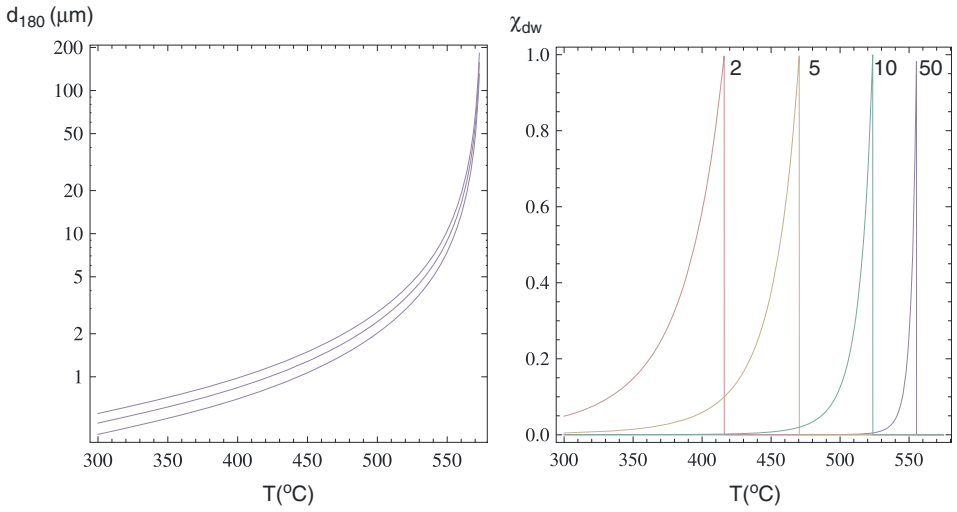

Figure 5. (a) Approximate width of 180° Bloch walls in magnetite as a function of temperature. This width determines the minimal size for particles which contribute susceptibility due to domain wall movement at the given temperature. (b) Approximate relative susceptibility variation due to domain-wall motion for four particle sizes in magnetite. The numbers indicate approximate particle diameter in micrometers.

ferrimagnetic crystals is so small that they contain only a small number of atoms in at least one dimension, this can lead to a considerable reduction of the particles' ordering temperature T_C(particle) as compared to the T_C of the bulk material. A detailed theoretical evaluation of this effect is given in *Shcherbakov et al.* [2012]. In this case, the magnetic susceptibility reflects the lowered T_C due to the particle size distribution. For magnetite this becomes a noticeable effect when at least one of the particle dimensions is less than ≈15 nm. The reduction in T_C, e.g., for spherical magnetite grains of 10 nm diameter is about 30 K, and for smaller grains becomes rapidly larger [*Sadeh et al.*, 2000].

[41] If the particles are large enough to essentially order at the bulk T_C, they still are superparamagnetic in the range between T_C and their respective blocking temperatures T_B. In this temperature interval the initial magnetic susceptibility is dominated by thermal fluctuations of the relatively large ordered particles. This superparamagnetic susceptibility is considerably more prominent than the para-effect due to the variation of M_s with field. Thereby the peak of the total magnetic initial susceptibility will be lowered to T_B, clearly below T_C.

[42] A calculation of the peak position for magnetite can be based on a single-domain particle of volume v, and shape anisotropy with demagnetizing factor $1/3 \le N \le 2/3$. Its energy barrier to magnetization changes then is

$$E_b = \mu_0 N M_s(T)^2 v, \tag{28}$$

leading to a relaxation time

$$\tau = \tau_0 \exp\left(\frac{E_b}{2k_B T}\right), \tag{29}$$

where $\tau_0 \approx 10^{-9}$ s is the spin relaxation time, and k_B is the Boltzmann constant [*Shcherbakov and Fabian*, 2005]. For susceptibility measurements a particle is considered blocked with $\chi_{SP} = 0$ if the critical relaxation time is more than $\tau = 0.1 - 1$ s, or

$$\log(\tau/\tau_0) \ge 20. \tag{30}$$

[43] With $M_s(T) \approx M_{s,0}(1 - T/T_C)^{1/2}$, and by defining a particle temperature $T_v = \mu_0 N \ M_{s,0}^2 v/(40 k_B)$, the blocking temperature T_B from (30) after substituting (29) and (28) yields

$$T_B \approx \frac{1}{\frac{1}{T_C} + \frac{1}{T_v}}, \tag{31}$$

T_B corresponds to the Hopkinson peak temperature T^* of magnetic susceptibility above which the volume specific superparamagnetic susceptibility

$$\chi_{SP}(T) = \frac{\mu_0 M_s(T)^2 v}{3 k_B T}, \tag{32}$$

is the dominant contribution. In Figure 6 this peak temperature is plotted as a function of diameter for spherical magnetite particles.

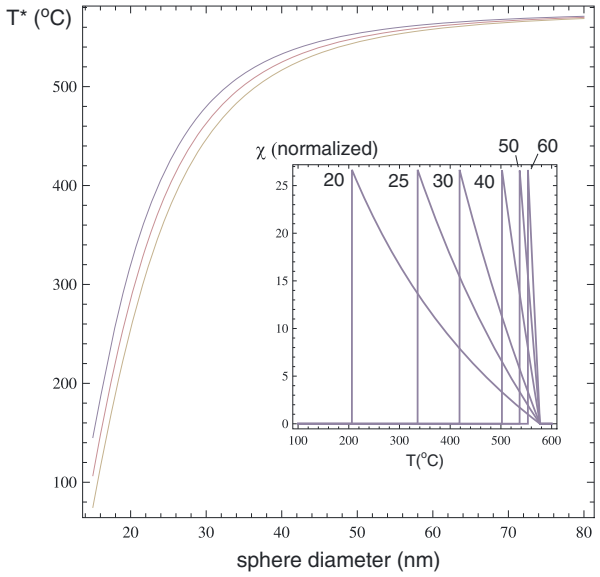

Figure 6. Approximate peak temperature T^* for the Hopkinson peak in magnetite as estimated from (31). Volume is transferred to an equivalent spherical diameter, and the error band takes into account a range of $\tau = 0.01 - 1$ s and of the demagnetizing factor $N = 1/4 - 1/3$. The inset shows the superparamagnetic susceptibility $\chi_{SP}(T)$ for six grain sizes that sets in at the blocking temperature (vertical line) and decreases with increasing temperature toward T_C according to (32). Numbers indicate the grains' spherical diameters in nanometers.

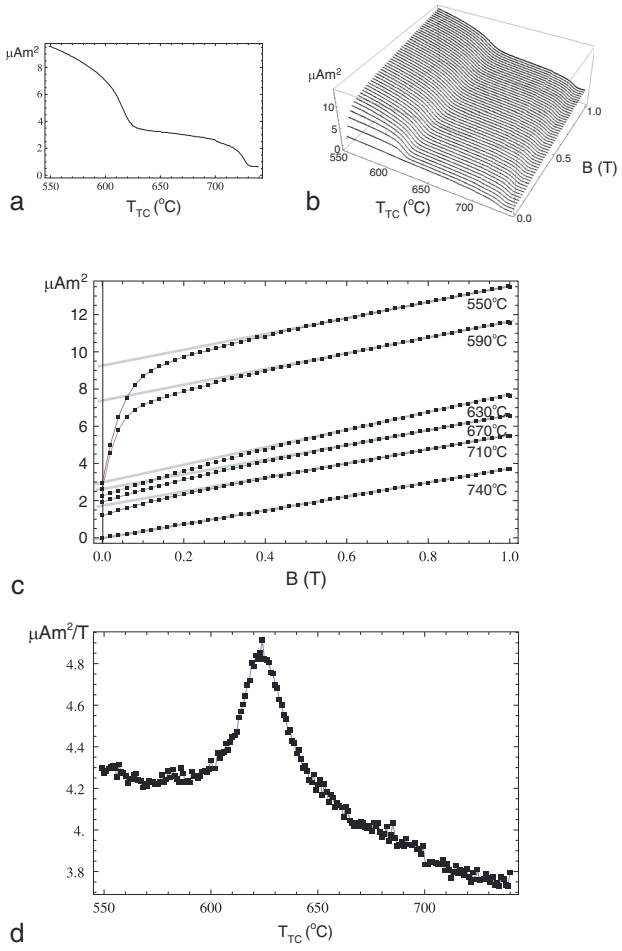

Figure 7. High-temperature calibration measurements for a hematite-magnetite sample. At the thermocouple the temperature T_{TC} is measured. The offset between sample temperature and T_{TC} is calibrated to the Curie points of magnetite at 578°C and hematite at 680°C. (a) The result of a classical high-temperature magnetization measurement $M(H,T)$ for $H = 500$ mT. (b) Dense sequence of $M_{si}(H,T)$ measurements with $\Delta T = 1$°C and $\Delta H = 50$ mT. Measuring Figure 7b requires approximately the same time as measuring Figure 7a. (c) Individual $M_{si}(H,T)$ curves at different thermocouple temperatures (indicated). For $T_{TC} = 550°, 590$°C, the sample temperature apparently lies below the Curie temperature of magnetite. For $T_{TC} = 630°, 670°, 710$°C, it lies between magnetite and hematite, and for $T_{TC} = 740$°C above the Néel temperature of hematite. Gray lines indicate the high-field tangents, from which a high-field slope $\chi_{hf}(T_{TC})$ and an estimate of $M_s(T_{TC})$ can be obtained. (d) Plotting all high-field slopes $\chi_{hf}(T_{TC})$ shows a clear maximum near the Curie temperature of magnetite, but does not mark the antiferromagnetic ordering of hematite.

4. A New Procedure to Improve Curie Point Measurements

[44] In this section an improved technique for fast high-temperature measurements, using a VSM, is described. The common measurement scheme, as, e.g., implemented in the PMC Inc. HT-VSM and most Curie balances, is to apply a constant field H during heating and cooling, and to measure the values $M(H,T)$. A typical result of this procedure is shown in Figure 7a for a calibration sample containing magnetite and hematite (T_{TC} is the temperature at the thermocouple). To minimize thermal hysteresis, and to achieve an accurate value for T_C, the temperature changes must be slow enough to permit thermal equilibration of the sample at each temperature step. Hence, even for relatively small samples, a full heating curve up to 600–700°C requires a measurement time of 30–60 min.

[45] The proposed new method uses the inevitable waiting time at each temperature step to measure not only a single value, but a full magnetization curve at different field values. For a high-temperature VSM (PMC Inc.), it is convenient to measure a sequence of saturation-initial curves $M_{si}(H,T)$ [*Fabian and von Dobeneck*, 1997; *Fabian*, 2003].

[46] At each temperature step T_i to T_{i+1}, the sample is heated in zero field to T_{i+1}. To minimize

measuring time, the field is then increased in relatively large steps (e.g., $\Delta H = 50$ mT) to the maximum field (e.g., 1.5 T). Besides the initial saturation, which took place at T_i, this procedure essentially measures $M_{si}(H, T_{i+1})$ at temperature T_{i+1}. The field is switched off before further heating. Instead of the single curve shown in Figure 7a, this procedure returns the two-dimensional data set as in Figure 7b.

[47] If the temperature step is small (e.g., $\Delta T = 1 - 3$°C), $M_{rs}(T_i)$ can be determined to good approximation by the first measurement of $M_{si}(H, T_i)$ at $H = 0$. Otherwise, the average $(M_{si}(0,T_{i+1}) + M_{si}(0,T_{i-1}))/2$ could provide a better estimate of $M_{rs}(T_i)$. When heating rate, temperature step ΔT, and measurement time (through ΔH) for each $M_s(T)$-curve are appropriately chosen, this M_{si} measurement requires the same total measurement time as a common $M(H, T)$ measurement with the same overall heating rate. However, by acquiring many data points in different fields, a more sophisticated data analysis becomes possible.

[48] Figure 7 visualizes how the measured $M_{si}(T)$ curves for several temperatures increase the information obtained during one heating cycle. A linear fit of the high-field region of the $M_{si}(H, T_i)$ curve at temperature T_i has the equation $M_s(T_i) + \chi_{hf}(T_i)H$, where $\chi_{hf}(T_i)$ is the high-field susceptibility, determined by paramagnetism and diamagnetism, the para-effect, or field-induced spin canting. These fits are represented by gray lines in Figure 7c and yield estimates for $M_s(T_i)$ and $\chi_{hf}(T_i)$, respectively. Due to the small temperature step ΔT, nearly continuous curves of $M_s(T)$, $M_{rs}(T)$ and $\chi_{hf}(T)$ can be derived. Figure 7d shows that for the magnetite-hematite calibration sample a clear peak in $\chi_{hf}(T)$ for magnetite indicates the para-effect close to the Curie point, while the antiferromagnetic ordering transition for hematite shows no discernible peak.

4.1. Field-dependent $M(T)$ Curves

[49] Using temperature-dependent measurements of quarter hysteresis loops it is possible to construct induced magnetization $M(H,T)$ curves for any value of H. In Figure 8a this is done for an Icelandic basalt containing fine-grained magnetite. Using this data set, it is also possible to construct a plot of m^3/h, which according to equation (8) in case of a pure magnetic mineralogy at T_C should be constant as a function of h. Figure 8b shows that this version of the Arrott plot gives a precise estimate of $T_C \approx 574$°C for this sample. To compare this with estimates from other determinations, Figure 8c plots m', m'', high-field susceptibility, $M_s(T)$, and $M_{rs}(T)$. In agreement with Landau theory, the minimum of m', or the zero of m'', appears to be independent of the applied field within measurement precision. However, the position of this minimum is closer to 571°C, and thus slightly lower than the estimate from the Arrott plot. In any case, the maximum of m'' varies with field intensity and always lies about 10–15°C above T_C. The lower panel shows that the two-tangent method of *Grommé et al.* [1969] essentially coincides with the peak determination of m'' and correspondingly overestimates T_C. It should be noted that the measured $M_{rs}(T)$ curve does not fully vanish at $T_C \approx 574$°C. This residual remanence is probably due to mineralogical inhomogeneity within this natural sample, leading to a distribution of Curie points as sketched in Figure 1. The vanishing of remanent magnetization sensitively traces the upper end of the T_C distribution, while the other methods record a lower average T_C value. The peak of $\chi_{hf}(T)$ in Figure 8c lies some 5°C above T_C, in agreement with Landau theory. The advantage of this Landau peak is that it also can be found in samples containing several magnetic minerals, as in Figure 9. Here it very accurately delimitates the Curie point of the magnetite phase, which lies 30–40°C above the maximum of the initial susceptibility.

5. Discussion and Conclusions

5.1. Discussion

[50] The aim of this article is twofold. It gives an overview of the relevant physical mechanisms that influence the classic methods of Curie point temperature determination, and introduces an improved measurement method to infer several magnetization parameters in one single high-temperature run.

[51] By evaluating previous work, including our own, we became aware that for the last decades the methods used for determining Curie points in rock and paleomagnetism were not based on a solid physical foundation, and mostly systematically overestimate T_C. The reason why this has not been improved previously is that for most practical purposes the errors are negligible, and that the calibration of the instrumentation is based on similarly overestimated Curie point temperatures. Thereby, the numerical values reported were not too far off from the correct values. However, in cases where the difference between the calibration point and the measured T_C is large, the literature certainly contains Curie point temperatures off by tens of degrees. Serious problems occur in studies which

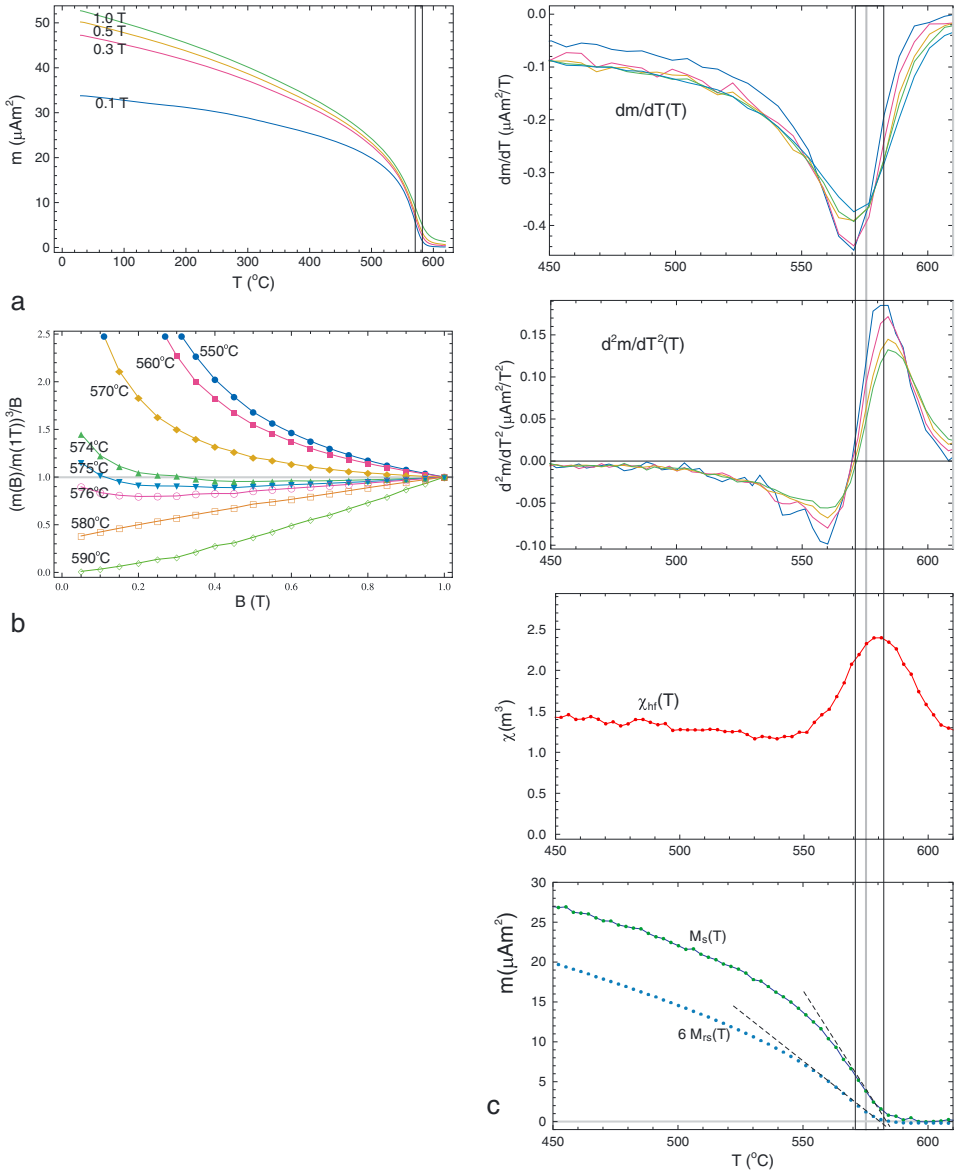

Figure 8. High-temperature measurements on an Icelandic basalt ST107A, containing fine-grained magnetite. (a) Induced magnetization $M(B,T)$ for different values of the inducing field B. (b) Plots of $(M(B,T)/M(1,T))^3/B$ versus B for different temperatures. Landau theory predicts that this plot should yield the constant value 1 for $T = T_C$. (c) Derivatives, curvatures, high-field susceptibility $\chi_{hf}(T)$, $M_s(T)$, and $M_{rs}(T)$ yield different estimates of T_C. The black vertical lines define the temperature interval between zero and maximum of the second derivative, while the gray vertical line indicates $T_C = 574°C$ as derived from Figure 8b.

compare Curie point temperatures obtained by different physical measurements, like susceptibility and in-field measurements. Many of these results should be reevaluated.

[52] The new measurement scheme presented here has several advantages over a usual high-field measurement. It efficiently uses the waiting time for thermal equilibration to determine $M_s(T)$, $M_{rs}(T)$, and $\chi_{hf}(T)$ in one run. By interpolation one can construct all curves $M(H,T)$, and generate Arrott plots. Especially the measurement of $\chi_{hf}(T)$ has not been used previously to determine T_C, but proves useful to distinguish ferrimagnetic from (weak) antiferromagnetic phases.

5.1.1. The Role of Paramagnetic Susceptibility

[53] For rock magnetic applications it is of interest to estimate at which concentration of an admixed paramagnetic material the determination of T_C for

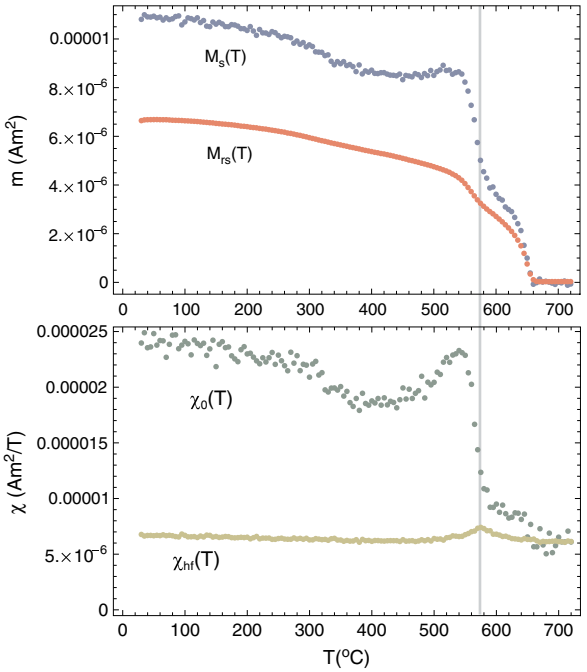

Figure 9. High-temperature measurements on a sample containing magnetite and hematite (Tenant Creek, Australia). The top panel shows the extrapolated $M_s(T)$ and the approximate $M_{rs}(T)$ from the measured $M_{sf}(H,T)$ curves. The bottom panel contains the low- and high-field magnetic susceptibilities inferred from the same data set.

the ferrimagnetic phase becomes problematic. The magnetization of the paramagnetic material near the Curie point of the ferrimagnetic phase is

$$M_p(T_C) = \frac{g^2\, S(S+1)\mu_B^2 n}{3\, k_B\, T} H = \frac{g\,(S+1)\mu_B\, n}{3} h, \qquad (33)$$

where h is defined by (18). Using the ferrimagnetic magnetization given by (8) with a concentration c of Fe ions yields the total magnetization

$$M(T_C) = \mu_B\, n \left(cm + (1-c)\frac{(S+1)}{3S} h \right) \qquad (34)$$

$$= \mu_B\ n h^{1/3} \left(c + (1-c)\frac{(S+1)}{3\,S} h^{2/3} \right). \qquad (35)$$

[54] The two contributions from paramagnetic and ferrimagnetic materials are approximately of the same size, when $c \approx h^2/3$, which for high fields ($h = 10^{-3}$) means $c < 1\%$. This result explains why the determination of T_C from a single high-field $M(H,T)$ curve can be seriously influenced or made impossible by a coexisting paramagnetic mineral that contains 100–1000 times more Fe than the ferrimagnetic mineral, especially if the latter is inhomogeneous, with Curie point temperatures distributed over a few degrees Celsius.

[55] In this case again the new method has the advantage that it determines an $M_s(T)$ curve that, due to extrapolation to $H = 0$, is less affected by the paramagnetic phase.

[56] When looking at the initial susceptibility, a relative concentration of $c \approx 0.01 - 0.1\,\%$ of ferrimagnetic minerals marks a practical detection limit, because at this point the paramagnetic susceptibility exceeds the ferrimagnetic, and the onset of ordering cannot be identified reliably.

5.2. Conclusions

[57] The outcome of the Curie point determination depends on grain size and on the measurement method. The approximate grain sizes given below are values for magnetite, but their order of magnitude applies similarly to many magnetic minerals.

(1) For extremely fine grains with sizes of 1–20 nm, the ordering temperature T_{ord} lies below the bulk T_C by about 1–100°C, depending on size [*Shcherbakov et al.*, 2012]. In this case, any measurement method yields an incorrect result, if the measured ordering temperature is interpreted as a bulk T_C for a particular mineral.

(2) Particles with size up to some 100 nm behave superparamagnetically above their blocking temperature, which can be several tens to hundreds degrees below T_C. For these grains, the peak of weak field susceptibility (Hopkinson peak) corresponds to this average blocking temperature. Only strong field measurements provide the bulk $M_s(T)$ curve indicating T_C by the minimum of dM_s/dT. They may also show the Landau peak of dM_s/dH slightly above T_C (Figure 2b).

(3) Grains with single-domain blocking temperature close to T_C. In these grains, the Hopkinson peak lies within a few degrees of T_C. In a strong field the minimum of dM_s/dT corresponds to T_C and the Landau peak of dM_s/dH lies only 5–10° above T_C. This peak theoretically occurs also in weak-field susceptibility, but might be completely buried under the step-like increase of the induced magnetization generated by the rotation of vectors **m** from the easy axes directions. The contributions of superparamagnetic and rotational susceptibilities are

$$\chi_{SP} = \frac{M_s^2\, V}{3\, k_B\, T}, \qquad (36)$$

and

$$\chi_{rot} = \frac{M_s^2 V}{6K}. \quad (37)$$

Their ratio $\chi_{SP}/\chi_{rot} = 2KV/(k_B T)$ increases on cooling, and by definition assumes a value of about 50 at the blocking temperature T_b. Hence, χ_{SP} dominates over χ_{rot} until more than 98% of the particle volume is thermally blocked.

[58] (4) Multidomain grains. In a strong field again the minimum of $dM_s dT$ indicates T_C, and the Landau peak of dM_s/dH lies only 5–10° above T_C. In weak fields the dominant magnetization change is due to domain wall movement. Close below T_C, domain walls become very large due to rapidly vanishing magnetocrystalline anisotropy. Other inhomogeneous magnetization structures, like multivortex structures, may emerge. These structures are also easily moved by an external field and produce a susceptibility similar to that of domain wall movement.

[59] In summary, strong field measurements always produce a minimum of dM_s/dT at T_C, and for ferrimagnetic minerals a Landau peak of dM_s/dH slightly above T_C, while weak-field magnetic susceptibility rather yields a step-like increase with maximum below T_C. For superparamagnetic grain sizes, the downward shift of the maximum can be several tens of degrees. If the particles contain only few atomic layers, surface effects decrease the average exchange coupling and can dramatically lower the ordering temperature.

Appendix A

Initial Susceptibility Due to Rotation Against Anisotropy Near the Curie Point

[60] We start from equations (12), (19), and (20). The measured magnetization in a field h is the projection on the field direction averaged over all directions of anisotropy axes.

$$m_{avg}(h) = \int_0^{\pi/2} m(\phi, h)\ \cos\theta(\phi, h)\ \sin\ \phi\, d\phi. \quad (A1)$$

[61] The susceptibility $\chi_0 = (dm_{avg}/dh)(0)$ is then obtained from

$$\chi_0 = \lim_{h\to 0} \int_0^{\pi/2} \left(\frac{dm}{dh}\cos\theta - m\ \sin\theta \frac{d\theta}{dh}\right) \sin\ \phi\, d\phi. \quad (A2)$$

[62] From the derivatives of (19) and (20) with respect to h one obtains for $h = 0$ with $\theta(\phi,0) = \phi$

$$\left(\alpha\tau + 3\beta m^2\right)\frac{dm}{dh} = \cos\theta, \quad (A3)$$

$$\frac{km}{2} 2\frac{d\theta}{dh} + \sin\theta = 0. \quad (A4)$$

[63] In the first expression one can insert the relations $m^2 = -\alpha\tau/\beta$, $\cos\theta = \cos\phi$, and in the second one can use $\sin\theta = \sin\phi$ to obtain

$$\frac{dm}{dh} = -\frac{\cos\phi}{2\alpha\tau}, \quad (A5)$$

$$\frac{d\theta}{dh} = -\frac{\sin\phi}{km}. \quad (A6)$$

[64] Inserting this into (A2) and again replacing θ by ϕ the equation simplifies to

$$\chi_0 = \int_0^{\pi/2} \left(-\frac{\cos^2\phi}{2\alpha\tau} + \frac{\sin^2\phi}{k}\right)\sin\ \phi\, d\phi. \quad (A7)$$

[65] This integral is now readily evaluated and yields

$$\chi_0 = -\frac{1}{6\alpha\tau} + \frac{2}{3k}. \quad (A8)$$

Acknowledgments

[66] The research was supported by grant 189721 from the Research Council of Norway (Nanomat Program) in the EU Matera Program. VSM measurements have been performed using visiting research fellowships to the Institute of Rock Magnetism (IRM), University of Minnesota, U.S.A., which is supported by an NSF Instruments and Facilities Grant. We gratefully acknowledge thoughtful comments by Mike Jackson, Bruce Moskowitz, and an anonymous reviewer.

References

Ade-Hall, J., R. Wilson, and P. Smith (1965), The petrology, Curie points and natural magnetizations of basic lavas, *Geophys. J.*, *9*, 323–336.

Arrott, A. (1957), Criterion for ferromagnetism from observations of magnetic isotherms, *Phys. Rev.*, *108*, 1394–1396.

Arrott, A., and J. E. Noakes (1967), Approximate equation of state for nickel near its critical temperature, *Phys. Rev. Let.*, *19*, 786–789.

Bertotti, G. (1998), *Hysteresis in Magnetism*, Academic Press, San Diego.

Collinson, D. W. (1993), *Methods in Rock Magnetism and Palaeomagnetism*, 1st ed., Chapman and Hall, London.

Dunlop, D. J., and O. Özdemir (1997), *Rock Magnetism*, Cambridge University Press, Cambridge.

Fabian, K. (2003), Some additional parameters to estimate domain state from isothermal magnetization measurements, *Earth Planet. Sci. Lett.*, *213*, 337–345.

Fabian, K., and von T. Dobeneck (1997), Isothermal magnetization of samples with stable Preisach function: A survey of hysteresis, remanence and rock magnetic parameters, *J. Geophys. Res.*, *102*, 17659–17677.

Fletcher, E. J., and W. O'Reilly (1974), Contributions of Fe^{2+} ions to the magnetocrystalline anisotropy constant K_1 of $Fe_{3-x}Ti_xO_4$ ($0 < x < 0.1$), *J. Phys. C: Solid State Phys.*, *7*, 171–178.

Grommé, C. S., T. L. Wright, and D. L. Peck (1969), Magnetic properties and oxidation of iron-titanium oxide minerals in Alae and Makaopuhi lava lakes, Hawaii, *J. Geophys. Res.*, *74*, 5277–5294.

Heider, F., A. Zitzelsberger, and K. Fabian (1996), Magnetic susceptibility and remanent coercive force in grown magnetite crystals from 0.1 μm to 6 mm, *Phys. Earth Planet. Inter.*, *93*, 239–256.

Holstein, T., and H. Primakoff (1940), Field dependence of the intrinsic domain magnetization of a ferromagnet, *Phys. Rev.*, *58*, 1098–1113.

Lagroix, F., S. K. Banerjee, and B. M. Moskowitz (2004), Revisiting the mechanism of reversed thermoremanent magnetization based on observations from synthetic ferrian ilmenite ($y = 0.7$), *J. Geophys. Res.*, *109*, doi:10.1029/2004JB003076.

Landau, L. D., and E. M. Lifshitz (1980), *Statistical Physics, 3rd ed. Course of Theoretical Physics, vol. 5*. Pergamon Press, Oxford.

Leonhardt, R. (2006), Analyzing rock magnetic measurements: The RockMagAnalyzer 1.0 software, *Comp. Geosci.*, *32*, 1420–1431.

Moskowitz, B. M. (1981), Methods for estimating Curie temperatures of titanomaghemites from experimental $j_s - t$ data, *Earth Planet. Sci. Lett.*, *53*, 84–88.

Moskowitz, B. M. (1993), High-temperature magnetostriction of magnetite and titanomagnetites, *J. Geophys. Res.*, *98*, 359–371.

Néel, M. L. (1948), Propriétés magnétiques des ferrites; ferrimagnétisme et antiferromagnétism, *Ann. Phys.*, *33*, 137–198.

Petersen, N., and U. Bleil (1982), Curie temperature, in *Landolt-Börnstein: Numerical Data and Functional Relationships in Science and Technology* edited by G. Angenheister, SpringerMaterials: The Landolt-Börnstein database. DOI: 10.1007/10201909_76.

Petrovský, E., and A. Kapička (2006), On determination of the Curie point from thermomagnetic curves, *J. Geophys. Res.*, *111*, doi:10.1029/2006JB004507, 1–10.

Sadeh, B., M. Doi, T. Shimizu, and M. Matsui (2000), Dependence of the Curie temperature on the diameter of Fe_3O_4 ultra-fine particles, *J. Mag. Soc. Jap.*, *24*, 511–514.

Scholz, W., K. Guslienko, V. Novosad, D. Suess, T. Schrefl, R. Chantrell, and J. Fidler (2003), Transition from single-domain to vortex state in soft magnetic cylindrical nanodots, *J. Magn. Magn. Mater.*, *266*, 155–163.

Shcherbakov, V. P., K. Fabian, N. K. Sycheva, and S. A. McEnroe (2012), Size and shape dependence of the magnetic ordering temperature in nanoscale magnetic particles, *Geophys. J. Int.*, *191*, 954–964.

Shcherbakov, V. P., and K. Fabian (2005), On the determination of magnetic grain-size distributions of superparamagnetic particle ensembles using the frequency dependence of susceptibility at different temperatures, *Geophys. J. Int.*, *162*, 736–746.

Shcherbakov, V. P., and M. Winklhofer (2010), Theoretical analysis of flux amplification by soft magnetic material in a putative biological magnetic-field receptor, *Phys. Rev. E*, *81*, 031921.

Tauxe, L. (1998), *Paleomagnetic Principles and Practice*, Kluwer, New York.

Träuble, H. (1966), Magnetisierungskurve und magnetische Hysterese, in: *Moderne Probleme der Metallphysik*, vol. 2, edited by A. Seeger, pp. 157–475, Springer-Verlag, Berlin Heidelberg, New York.

Williams, W., and D. J. Dunlop (1989), Three-dimensional micromagnetic modelling of ferromagnetic domain structure, *Nature*, *337*, 634–637.